



Article

# Meta-Inflammation and De Novo Lipogenesis Markers Are Involved in Metabolic Associated Fatty Liver Disease Progression in BTBR ob/ob Mice

Lucas Opazo-Ríos <sup>1,2,\*</sup>, Manuel Soto-Catalán <sup>1,†</sup>, Iolanda Lázaro <sup>3</sup>, Aleix Sala-Vila <sup>3</sup>,  
Luna Jiménez-Castilla <sup>1</sup>, Macarena Orejudo <sup>1</sup>, Juan Antonio Moreno <sup>4,5</sup>, Jesús Egido <sup>1,‡</sup>  
and Sebastián Mas-Fontao <sup>1,\*</sup>

<sup>1</sup> Renal, Vascular and Diabetes Research Laboratory, IIS-Fundación Jiménez Díaz, Universidad Autónoma de Madrid, Spanish Biomedical Research Centre in Diabetes and Associated Metabolic Disorders (CIBERDEM), 28040 Madrid, Spain; manuel.soto.catalan@gmail.com (M.S.-C.); luna.jimenez@quironasalud.es (L.J.-C.); macarena.orejudo@quironasalud.es (M.O.); jegido@quironasalud.es (J.E.)

<sup>2</sup> Facultad de Ciencias de la Salud, Universidad de Las Américas, Concepción-Talcahuano 4301099, Chile

<sup>3</sup> Hospital del Mar Medical Research Institute (IMIM), 08003 Barcelona, Spain; iolan.lazaro@gmail.com (I.L.); asala3@imim.es (A.S.-V.)

<sup>4</sup> Department of Cell Biology, Physiology and Immunology, University of Cordoba, 14004 Cordoba, Spain; jamoreno@fjd.es

<sup>5</sup> Maimonides Biomedical Research Institute of Cordoba (IMIBIC), UGC Nephrology, Hospital Universitario Reina Sofía, 14004 Cordoba, Spain

\* Correspondence: lopazo@udla.cl (L.O.-R.); smas@fjd.es (S.M.-F.); Tel.: +56-9204-63280 (L.O.R.); +34-9155-04899 (S.M.-F.)

† These authors contributed equally to this work.

‡ These authors contributed equally to this work.



Citation: Opazo-Ríos, L.;

Soto-Catalán, M.; Lázaro, I.; Sala-Vila, A.; Jiménez-Castilla, L.; Orejudo, M.; Moreno, J.A.; Egido, J.; Mas-Fontao, S. Meta-Inflammation and De Novo Lipogenesis Markers Are Involved in Metabolic Associated Fatty Liver Disease Progression in BTBR ob/ob Mice. *Int. J. Mol. Sci.* **2022**, *23*, 3965. <https://doi.org/10.3390/ijms23073965>

Academic Editor: Mi-Kyung Lee

Received: 17 February 2022

Accepted: 30 March 2022

Published: 2 April 2022

**Publisher's Note:** MDPI stays neutral with regard to jurisdictional claims in published maps and institutional affiliations.



**Copyright:** © 2022 by the authors. Licensee MDPI, Basel, Switzerland. This article is an open access article distributed under the terms and conditions of the Creative Commons Attribution (CC BY) license (<https://creativecommons.org/licenses/by/4.0/>).

**Abstract:** Metabolic associated fatty liver disease (MAFLD) is a hepatic manifestation of metabolic syndrome and usually associated with obesity and diabetes. Our aim is to characterize the pathophysiological mechanism involved in MAFLD development in Black Tan and brachyuric (BTBR) insulin-resistant mice in combination with leptin deficiency (ob/ob). We studied liver morphology and biochemistry on our diabetic and obese mice model (BTBR ob/ob) as well as a diabetic non-obese control (BTBR + streptozotocin) and non-diabetic control mice (BTBR wild type) from 4–22 weeks. Lipid composition was assessed, and lipid related pathways were studied at transcriptional and protein level. Microvesicular steatosis was evident in BTBR ob/ob from week 6, progressing to macrovesicular in the following weeks. At 12th week, inflammatory clusters, activation of STAT3 and Nrf2 signaling pathways, and hepatocellular ballooning. At 22 weeks, the histopathological features previously observed were maintained and no signs of fibrosis were detected. Lipidomic analysis showed profiles associated with de novo lipogenesis (DNL). BTBR ob/ob mice develop MAFLD profile that resemble pathological features observed in humans, with overactivation of inflammatory response, oxidative stress and DNL signaling pathways. Therefore, BTBR ob/ob mouse is an excellent model for the study of the steatosis to steatohepatitis transition.

**Keywords:** metabolic associated fatty liver disease; BTBR ob/ob; de novo lipogenesis; meta-inflammation

## 1. Introduction

Non-Alcoholic Fatty Liver Disease (NAFLD), is defined as an increased ectopic fat deposition (more than 5% of liver weight), independently of excessive alcohol consumption, hepatitis C infection, antiretroviral therapy, or chemotherapy drugs. It can range from simple steatosis to steatohepatitis, characterized by liver inflammation and hepatocyte ballooning, with or without fibrosis and described as liver cirrhosis [1,2]. This condition is usually

associated with obesity, systemic insulin-resistance and diabetes, being the most common cause of chronic liver disease, end-stage liver disease and liver transplantation worldwide [3,4].

The coexistence and synergistic links between the development of NAFLD and type 2 diabetes mellitus (T2DM) are well known [5,6]. Thus 56% of patients with T2DM present NAFLD [5]. But the relationship seems to be bidirectional [7,8] since in many cases NAFLD precedes and/or promotes the development of T2DM, meta-analyses have shown that the risk of developing T2DM in subjects with NAFLD doubles (HR 2.19) [9], also T2DM developments risk increasing with NAFLD severity. But also, as seen in the Korean population, if to the presence of NAFLD is added two other factors that coexist in many patients, such as obesity and insulin resistance, this risk increases up to 1400% (HR 14.13) [10]. Some authors distinguish between two different phenotypes of NAFLD: 'genetic' vs. 'metabolic'. Therefore, metabolic NAFLD would be the phenotype associated with the development of T2DM, and its main characteristic is the presence of insulin resistance that precedes and originates the accumulation of lipids in the liver [11]. As this phenotype constitutes the most frequent clinical presentation, in 2020 and international expert panel from 22 countries proposed a novel definition of metabolic associated fatty liver disease (MAFLD) to replace "metabolic" NAFLD. Thus MAFLD is clinically defined by presence of obesity/overweight or T2DM or at least two metabolic risk abnormalities (hypertension, insulin-resistance, hyperlipidemia, CRP > 2 mg/L among other things) [12], however, understanding of the underlying mechanisms remains limited [13,14]. Insulin resistance has also been acknowledged as a MAFLD predictor in childhood, and both entities associate to an increase cardiometabolic burden [15,16], although the causal relationship among them seems more complex [17], as observed in young obese. In this context, the recent identification of new mediators that trigger inflammation, oxidative stress or lipotoxicity in the transition from steatosis to steatohepatitis, may be useful to prevent or retard the progression of the disease [18].

Genetic, chemical and dietary factors are the main inducers of MAFLD in preclinical models [19]. Among the most employed MAFLD genetic models are those derived from the ob/ob mutation (leptin deficiency), being C57BL/6J ob/ob mice the most widely known. Another ob/ob model, in which the leptin mutation is found in an insulin-resistant BTBR strain, is the BTBR ob/ob, leading to early T2DM development and maintenance of hyperglycemia, compared with other ob/ob models, as the animal become overweight/obese. This model is known due to its unique susceptibility to develop diabetic complications [20–23]. BTBR ob/ob strain background is a potent accelerator of kidney pathology, depicting histopathological lesions similar to those observed in human diabetic kidney disease [20]. Liver involvement in this model was also studied at early weeks and the authors concluded that the model was resistant to steatosis [24]. However, based on our observation that the livers of these animals did show indeed hepatomegaly at 12 weeks, we set out to characterize the hepatic involvement of the BTBR ob/ob mice, as well as, the pathophysiological mechanisms involved in MAFLD progression by using the BTBR ob/ob mouse model, in the presence/absence of obesity and hyperglycemia.

## 2. Results

### 2.1. Characterization of the Metabolic Factors Involved in Early MAFLD Progression in BTBR ob/ob Model

BTBR ob/ob mice cannot be differentiated phenotypically from their littermates BTBR WT until 4 to 6 weeks of life. Animals were fed with standard chow (used throughout the study) and changes in body weight and non-fasting glycemia were already detected from 4th and 6th week of life, respectively (Figure 1A,B). After 12 weeks of life, liver triglycerides content (Figure 1D), as well as serum metabolic parameters, were increased in BTBR ob/ob mice vs. BTBR WT, with significant changes in all studied variables (Table 1).

Macroscopical differences were observed in the liver of BTBR ob/ob mice during the first 12 weeks of life, mainly hepatomegaly (Figure 1C). Histopathologically, microvesicular steatosis was evident from week 6, progressing to macrovesicular during the following

weeks (Figure 1F). At the 12th week of life, inflammatory clusters/foci and hepatocellular ballooning were also detectable (Figure 1G).

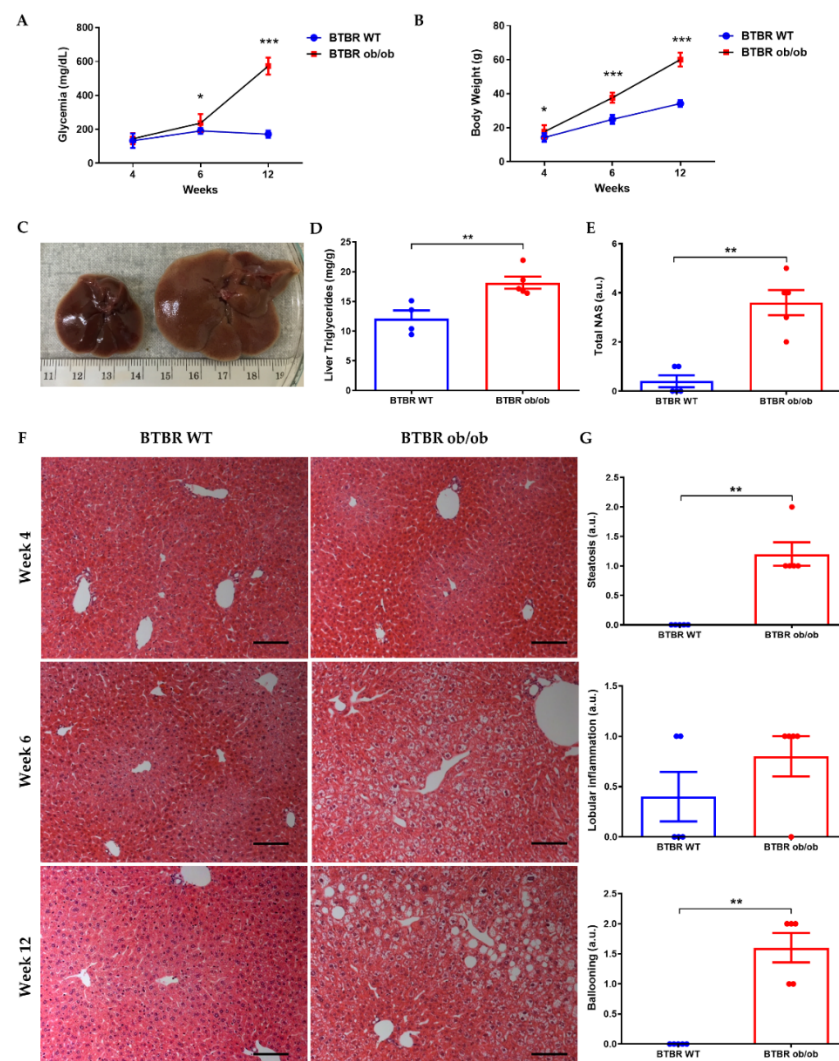


**Figure 1. Progression of liver steatosis from weeks 4 to 12.** Non-fasting glycemia (A) and body weight (B) of BTBR WT and BTBR ob/ob mice at 4, 6 and 12 weeks. (C) Macroscopic photograph of liver at 12 weeks in BTBR WT (left) and BTBR ob/ob mice (right). (D) Measurement of liver TGs at 12 weeks. (E) NAFLD activity score (NAS) assessment at 12 weeks (F) Representative H-E images of livers of BTBR WT (left) and BTBR ob/ob mice (right) showing steatosis progression (magnification 100×) from 4–12 weeks. (G) Semi-quantitative determination of steatosis, lobular inflammation and hepatocytes ballooning in livers of mice at 12 weeks. Data are shown as scatter dot plots and mean  $\pm$  SEM of each group ( $n = 5\text{--}6$  mice/group); \*  $p < 0.05$ , \*\*  $p < 0.01$ , \*\*\*  $p < 0.001$  vs. BTBR WT. Abbreviations: NAS: NAFLD activity score; a.u: arbitrary units.

## 2.2. Liver Inflammatory Cell Infiltration in the BTBR ob/ob Mice

The presence of inflammatory cells in the liver of BTBR ob/ob mice was analyzed at 12 weeks, including F4/80+ (monocytes/macrophages), CD3+ (T lymphocytes) and MPO+ (neutrophils). Even though no changes in F4/80+ cells between non-diabetic and diabetic mice were observed (Figure 2A,B), significant differences were detected in CD3+ T lymphocytes and MPO+ cells, meta-inflammation markers, observed in isolation at the interstitial level and forming part of inflammatory clusters (Figure 2C–F).

**Table 1. Metabolic and biochemical parameters in BTBR WT and BTBR ob/ob at 12 w.** Data are shown as Median (IQR). \*\*  $p < 0.01$ ; \*\*\*  $p < 0.001$  vs. BTBR WT. Abbreviations: AST: aspartate aminotransferase; ALT: alanine aminotransferase; AP: Alkaline Phosphatase; HDL-C: high-density lipoprotein cholesterol LDL-C: low-density lipoprotein cholesterol. & Undetectable. % n-fold change vs. BTBR WT.

Variables	BTBR WT	BTBR ob/ob	n-Fold Change %
AST (IU/L)	46 (39.75, 50.75)	76 (66.5, 58) **	1.65
ALT (IU/L)	27 (23, 30.25)	62 (52, 72.5) ***	2.29
AST/ALT ratio	1.66 (1.39, 2.16)	1.09 (1.02, 1.46)	-
AP (IU/L)	60.5 (54.75, 84.25)	146 (123.5, 163.5) ***	2.41
Total Cholesterol (mg/dL)	118 (103.3, 126.8)	215 (181, 275) **	1.82
Triglycerides (mg/dL)	123.5 (99.25, 129)	253.5 (192, 310.5) **	2.05
HDL (mg/dL)	101 (89.75, 109.3)	149 (141, 198) **	1.48
LDL (mg/dL)	0 (0, 0) &	19 (4, 26.5)	-

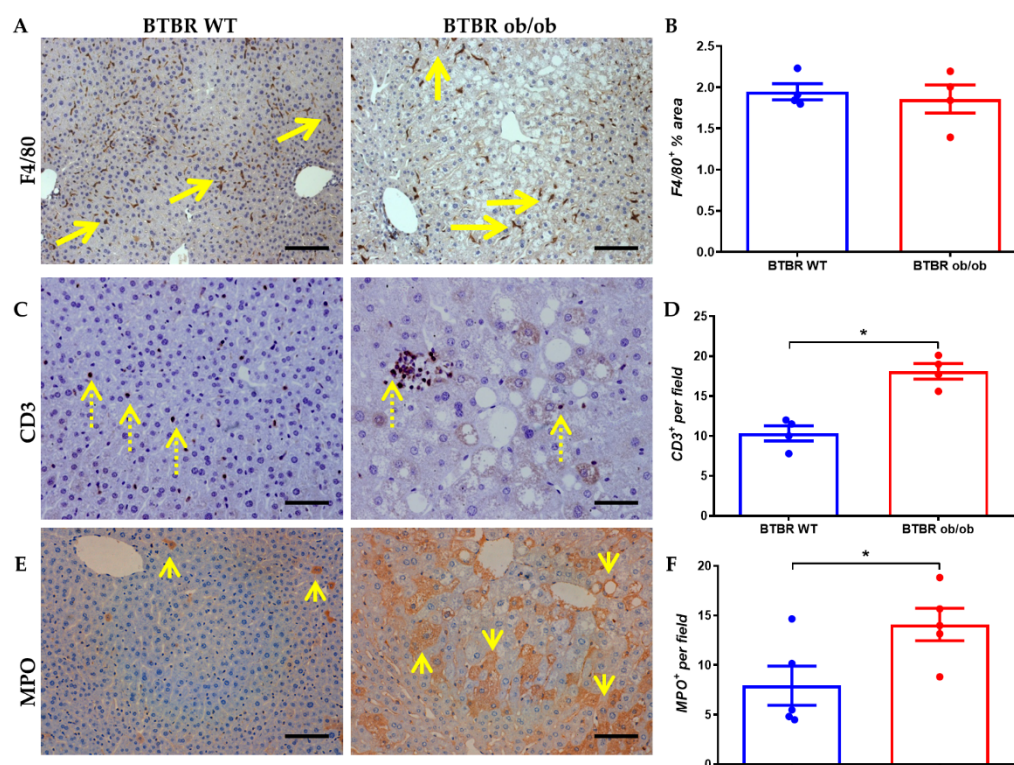


**Figure 2. Inflammatory infiltrate in BTBR WT (left) and BTBR ob/ob mice (right) at 12 weeks.** (A) Representative image of monocytes/macrophages infiltration (F4/80+ staining; long arrow) (magnification 100×), and F4/80+ area quantification (B). (C) Representative image (of lymphocytes T (CD3; dotted arrow) staining (magnification 200×) and its quantification (D). (E) Myeloperoxidase (MPO; short arrow) immunostaining (magnification 200×) and quantification of the positive cells per field (F). Data are shown as scatter dot plots and mean ± SEM of each group ( $n = 5$  mice/group); \*  $p < 0.05$  vs. BTBR WT.

### 2.3. Inflammatory, Oxidative Stress and Lipotoxic Markers in the Liver of BTBR ob/ob Mice

Intracellular signaling pathways related to inflammation, oxidative stress, and presence of lipotoxicity were activated at 12 weeks in our experimental model. At the immunohistochemical level, we observed increased JAK/STAT and NRF2 pathway activation (phosphorylation of the transcription factors STAT3 and NRF2, respectively) mainly in diabetic mice. Thus, pSTAT3 showed a clear cytoplasmic activation pattern, with minimal



nuclear translocation in hepatocytes of the diabetic mice (Figure 3A,B). NRF2 showed a constitutive pattern in hepatocytes, with a notable nuclear translocation (Figure 3C,D). Lipid peroxidation was higher in livers from BTBR ob/ob mice, with increased expression of 4-hydroxynonenal (4-HNE), a marker of lipid peroxidation (Figure 3E,F).

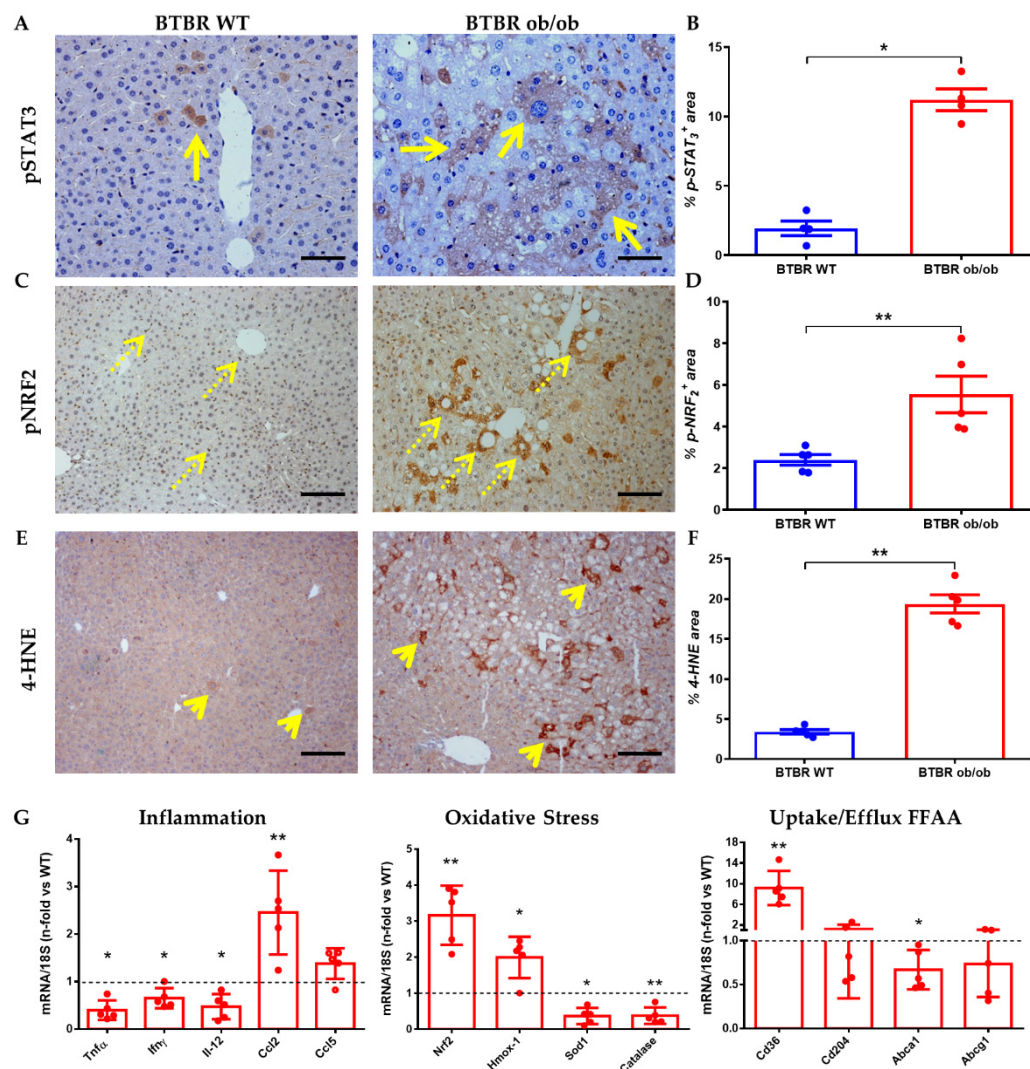


**Figure 3.** Comparison of inflammatory, oxidative stress and lipid markers between BTBR WT (left) and BTBR ob/ob (right) at 12 weeks. (A) Representative image of pSTAT3 (long arrow) immunostaining (magnification 200 $\times$ ) and (B) pSTAT3 activation quantification. (C) pNRF2 staining (dotted arrow) as oxidative stress response (magnification 100 $\times$ ) and area quantification (D). (E) 4-HNE staining (short arrow) as lipoperoxidation (magnification 100 $\times$ ) and its quantification (F). In the lower row (G) is shown mRNA expression of several inflammation (*Tnf $\alpha$* , *Ifn $\gamma$* , *Il-12*, *Ccl2* and *Ccl5*); oxidative stress (*Nrf2*, *Hmox-1*, *Sod-1* and *Catalase*) and lipid uptake/efflux (*CD36*, *CD204*, *ABCa1* and *ABCG1*) genes. Data are shown as scatter dot plots and mean  $\pm$  SEM of each group ( $n = 5$  mice/group); \*  $p < 0.05$ , \*\*  $p < 0.01$ , vs. BTBR WT.

Gene expression studies confirmed the presence of oxidative stress in BTBR ob/ob mice, since we observed a marked upregulation of *Nrf2* and its main effector HO-1 (*Hmox-1*), as well as downregulation of antioxidant enzymes such as *Sod1* and *Catalase*. BTBR ob/ob mice showed a lower liver expression of the inflammatory cytokines *Tnf $\alpha$* , *Ifn $\gamma$*  and *Il-12*, but a significant increase of the chemokine *Mcp-1* (*Ccl2*) (Figure 3G). Finally, scavenger receptors associated with fatty acid uptake (*Cd36*/*Cd204*) and efflux (*Abca1*/*Abcg1*) were also evaluated. An overexpression can be observed for *Cd36* whereas

Abca1 gene expression was downregulated. These results could indicate a possible intra-hepatic lipid accumulation in BTBR ob/ob, favoring the uptake and limiting the efflux of fatty acids.

#### 2.4. Long-Term Metabolic and Morphological Changes Associated to MAFLD

To assess the metabolic and morphological changes associated to MAFLD, livers from non-obese and non-diabetic (BTBR WT), non-obese and diabetic (BTBR-STZ) and obese and diabetic (BTBR ob/ob) mice were evaluated in a later stage (22 weeks). This approach was performed to differentiate between body weight- and hyperglycemia-dependent liver changes. As reported in Table 2, BTBR ob/ob mice showed a marked difference in body weight, liver weight, food and water intake, glycemia, alkaline phosphatase (AP), triglycerides, total cholesterol and LDL.

**Table 2. Metabolic and biochemical parameters in BTBR WT, BTBR-STZ and BTBR ob/ob at 22 weeks.** Data are shown as Median (IQR). \*  $p < 0.05$ ; \*\*  $p < 0.01$ ; \*\*\*  $p < 0.001$  vs. BTBR WT § non-parametric data: Mann-Whitney U test. Abbreviations: LW/BW: Liver weight/body weight ratio; AST: aspartate aminotransferase; ALT: alanine aminotransferase; AP: Alkaline Phosphatase; HDL-C: high-density lipoprotein cholesterol LDL-C: low-density lipoprotein cholesterol. & Undetectable. % n-fold change BTBR ob/ob vs. BTBR WT.

Variables	BTBR WT	BTBR STZ	BTBR ob/ob	n-Fold Change %
Water intake (mL/day)	5 (5, 6)	-	38 (32, 45) ***, §	7.60
Food intake (g/day)	6.7 (6.3, 7.8)	-	13.12 (12.17, 14.13) ***, §	1.96
Liver weight (g)	2.70 (2.60, 3.20)	-	6.19 (5.90, 6.82) ***	2.29
Body weight (g)	37 (36, 38)	31 (30, 34) ***, §	71 (69, 72) ***	1.91
LW/BW ratio	2.7 (2.5 3.2)	-	6.2 (5.9 6.9) *	2.30
Glycemia 22 week (mg/dL)	152 (149, 157)	350 (265, 380) ***, §	525 (493, 569) ***	3.45
AST (IU/L)	80 (64, 134)	88 (83, 95)	84 (74, 116) §	1.05
ALT (IU/L)	14 (11, 30)	38 (35, 42)	40 (35, 52) **, §	2.86
AST/ALT ratio	5.3 (3.9, 6.9)	2.0 (2.5 2.7)	2.0 (1.7, 2.7) ***	-
AP (IU/L)	38 (34, 54)	127 (108, 141)	97 (74, 113) ***	2.55
Total Cholesterol (mg/dL)	128 (121, 142)	112 (104, 120) **, §	204 (166, 233) ***	1.59
Triglycerides (mg/dL)	56 (53, 73)	134 (110, 151)	108 (98, 136) ***	1.93
HDL (mg/dL)	102 (98, 108)	96 (88, 103) **, §	158 (122, 175) ***	1.55
LDL (mg/dL)	10 (7, 27)	0 (0, 0) &	29 (24, 38) *, §	2.90

Histopathological analysis disclosed manifestations of MAFLD in BTBR ob/ob mice, including micro and macrovesicular steatosis, predominantly in zone 2 and 3, inflammatory clusters with intrasinusoidal neutrophil infiltration, isolated megakaryoblasts, glycogenated nuclei and hepatocellular ballooning (Figure 4C 1–5). The steatosis showed a characteristic location by functional zones. In non-diabetic mice, lipid droplets were exclusively detected in zone 3. The STZ model showed mainly microvesicular steatosis in zone 2 and 3, and marginal macrovesicular. Obese mice have a predominant macrovesicular steatosis in zones 2 and 3. The NAFLD activity score demonstrated a higher activity grade in BTBR ob/ob mice (Figure 4D). Although Periodic acid-Schiff (PAS) staining is used for glycoproteins/glycolipids detection, is widely utilized to evaluate glycogen storage in liver. BTBR WT exhibited a symmetrical pattern of intracellular positive PAS staining. Nevertheless, an irregular arrangement was observed in both diabetic livers (Figure 4B). These changes were mainly evidenced in zone 3 or pericentral zone in the hepatocytes of STZ-treated mice, while the obese and diabetic BTBR ob/ob mice disclosed an accentuated

location of steatosis in lipogenic zones, suggesting alterations of hepatocyte metabolism. Fibrosis was not observed (not shown).

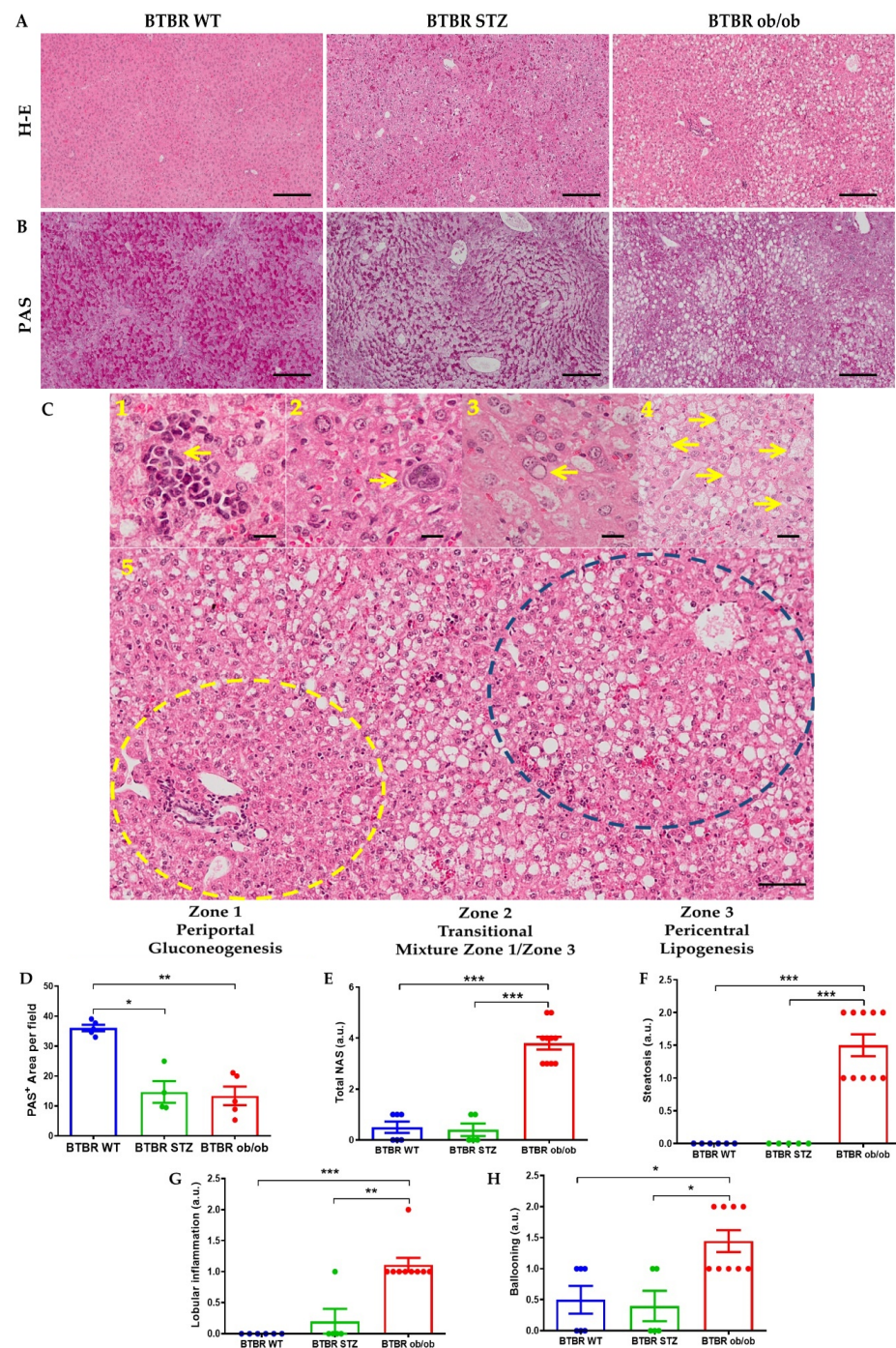


**Figure 4.** Liver histopathological changes at 22 weeks between BTBR WT, BTBR-STZ and BTBR ob/ob. Representative images of H-E (A) and PAS (B) staining in the 3 animal groups. (C) Major findings associated to MAFLD development: 1. Inflammatory clusters; 2. Isolated megakaryoblast; 3. Glycogenated nuclei; 4. Hepatocellular ballooning. 5. Steatosis distribution into 3 distinctive liver zones. (D) Quantification of positive Periodic Acid Schiff (PAS) staining, as glycogen liver deposition in BTBR WT, STZ and ob/ob mice. (E) Quantification of NAFLD activity score (total NAS) and its histopathological characteristics: (F) steatosis, (G) lobular inflammation and (H) hepatocytes ballooning. Data are shown as scatter dot plots and mean  $\pm$  SEM of each group ( $n = 5-8$  mice/group); \*  $p < 0.05$ , \*\*  $p < 0.01$ , \*\*\*  $p < 0.001$  vs. BTBR WT or BTBR-STZ.



### 2.5. Lipid Metabolism and Liver Lipidomics in the Experimental Model

BTBR ob/ob displayed a roughly 5-fold increase in total TG content in the liver as compared to BTBR WT, while when it was compared with STZ-treated BTBR mice this increase was even higher (Figure 5A). However, NEFA levels were only augmented in the liver and plasma of BTBR STZ mice (Figure 5B,C). To further explore the link between MAFLD and DNL, we analyzed the specific fatty acids that constitute the intrahepatic TG and NEFA fraction. In the hepatic TG fraction, focusing on those species which are the major products of DNL, BTBR ob/ob mice showed a significant increase in palmitic acid (C16:0; 562%), palmitoleic acid (C16:1n-7; 769%), stearic acid (C18:0; 130%), and oleic acid (C18:1n-9cis; 789%), compared to BTBR WT. These differences were even higher when comparing the results with the BTBR STZ mice (Figure 5D). This pattern was not observed for saturated fatty acids in NEFA fraction, since BTBR ob/ob mice showed a significant increase in palmitoleic (C16:1n-7; 104%), and oleic acid (C18:1n-9cis; 69%), compared with BTBR WT (Figure 5E). Detailed information about saturated fatty acids, mono-unsaturated fatty acids, and PUFA in TGs and NEFA fractions was described in Supplementary Figure S1.

The analysis based on the differences in fatty acids in the TG- and NEFA-fractions allowed us to discriminate each experimental models by using an Orthogonal Partial Least Squares Discriminant Analysis (oPLS-DA) (Figure 5F). In oPLS-DA, the component that best discriminated to the 3 different experimental groups was the presence of lipids associated with DNL (Supplementary Figure S1G). Furthermore, hierarchical clustering showed distinctive lipid profiles that associates with lipid composition in each one of the three groups (Figure 5G).

Different lipid ratios are used to assess the activity of the enzymatic pathways involved in their synthesis. Thus, DNL can be assessed by the ratio between palmitate (the main end product of DNL) and linoleate (whose origin is exclusively from the diet). The quantification of this ratio is 1.29 in BTBR WT animals, 2.67 in BTBR-STZ and 5.44 in BTBR ob/ob mice, with significant increases in the latter two vs. WT ( $p = 0.006$  and  $p < 0.001$ , respectively). Similarly, the ratios between saturated and unsaturated FA showed significant decreases (BTBR WT: 3.56; BTBR-STZ: 2.16; BTBR ob/ob: 2.43,  $p = 0.01$ ). Other elements measured were Elongase (oleate/palmitate); stearyl-coA desaturase indices (palmitoleate/palmitate and oleate/stearate) in both cases were significantly increased in BTBR ob/ob vs. WT (0.11 vs. 0.16  $p = 0.009$ ) and 7.12 vs. 27.7  $p < 0.0001$ ). In contrast delta-(5)-desaturase (D5D) index (arachidonate/dihomo- $\gamma$ -linolenate) significant variation was only observed in the STZ group (9.5 vs. 12.75  $p = 0.001$ ) [25].

### 2.6. Study of MAFLD Related Gene and Protein Expression in Liver from BTBR ob/ob Mice

In a next step, we analyzed the gene expression of makers associated with MAFLD progression. BTBR ob/ob mice showed a significant reduction in the main transcription factors related with lipo/glucogenic pathways, such as Srebp-1, Chrebp-1, Ppar $\alpha$ , with significant increase of Ppar $\gamma$  activity (Figure 6A). These results were confirmed at the protein level by western blot analysis (Figure 6G,H). Moreover, we also observed a significant increase in gene expression of enzymes related with DNL (Acc1, Fasn, Scd1) in BTBR ob/ob mice, whilst Dgat2 enzyme, that catalyzed the final step in TG synthesis, was downregulated. The expression of scavenger receptors associated with fatty acids uptake (Cd36, Cd204) was also upregulated, in contrast with the downregulation of markers associated with efflux (Abca1, Abcg1) or intracellular transporters (Fatp2) (Figure 6B,C). Oxidative stress markers Nfr2 and HO-1 were augmented whereas a decrease on genes associated with mitochondrial biogenesis was evidenced (Figure 6D). Besides, most inflammatory chemokines measured were upregulated (Ccl2, Cxcl10, Cx3cl1) with lower expression of cytokines (IL-15) or innate receptors (TLR4) (Figure 6E). Also, pro-fibrotic markers as TGF $\beta$ , CTGF and Gremlin (Figure 6F) were downregulated.



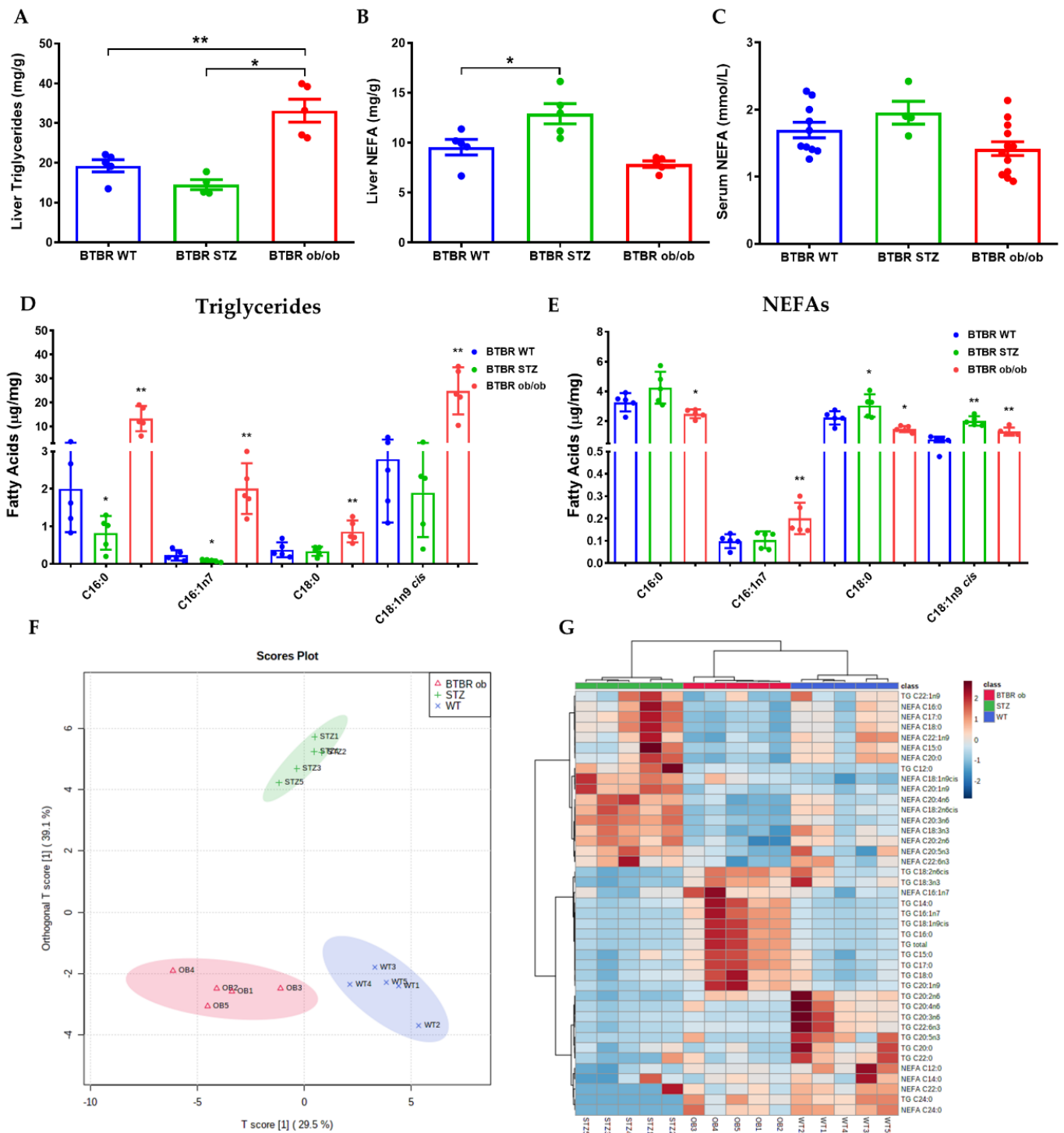


**Figure 5.** Lipid composition in liver at 22 weeks from BTBR WT (blue), BTBR–STZ (green) and BTBR ob/ob mice (red). Measurement of liver TGs (A), liver NEFAs (B) and serum NEFAs (C). Analysis by GC–MS of fatty acids, involved in de novo lipogenesis, from triglycerides (D) and NEFAs (E). (F) Orthogonal Partial Least Squares Discriminant Analysis (oPLS–DA) based on liver lipid composition data showing a clear separation between models. (G) Hierarchical clustering based on liver lipid composition showing the upregulated lipids (dark brown) and downregulated (dark blue) in each experimental group. Data are shown as scatter dot plots and mean ± SEM of each group ( $n = 5–8$  mice/group); \*  $p < 0.05$ , \*\*  $p < 0.01$  vs. BTBR WT or BTBR–STZ.

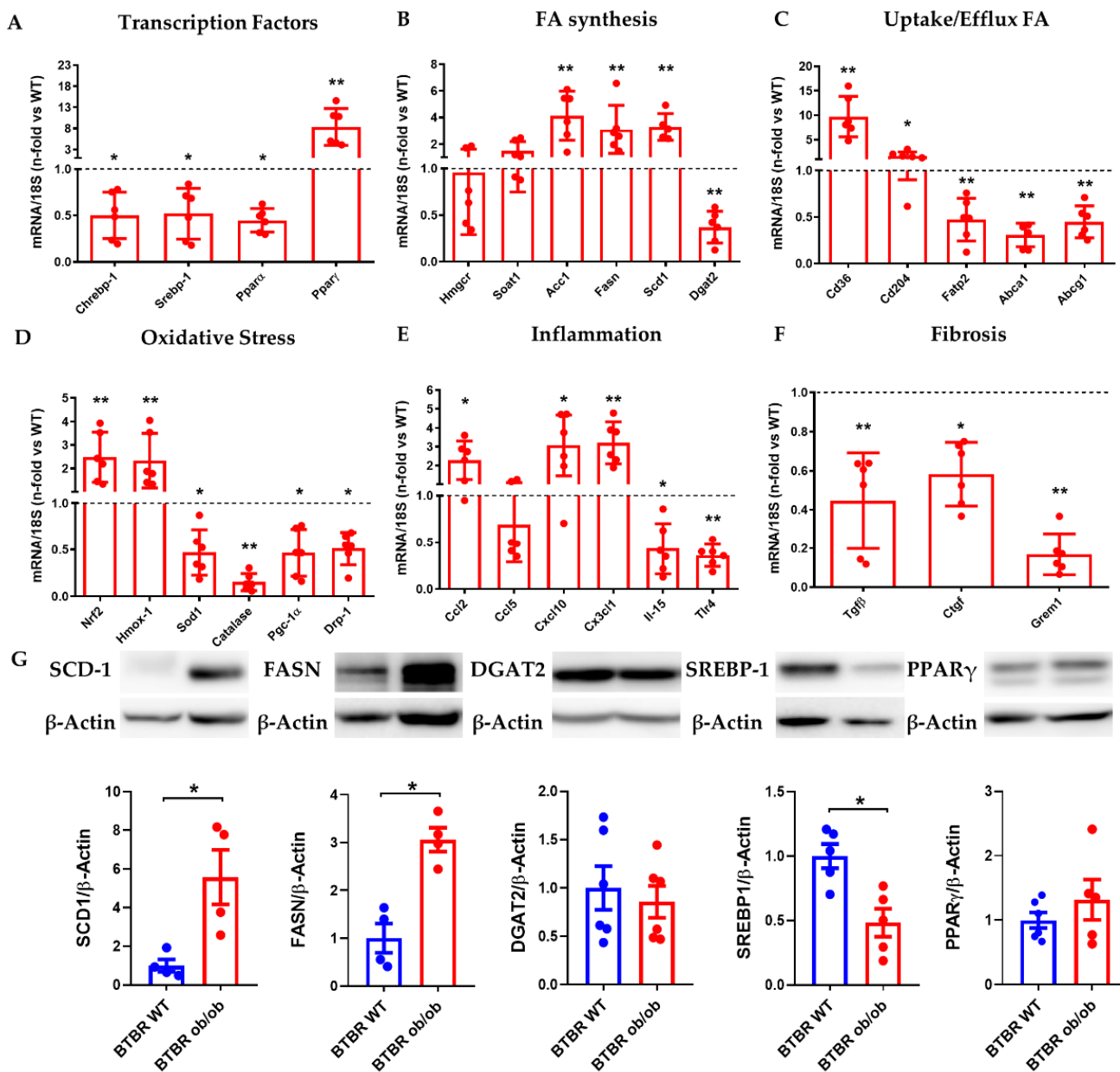


**Figure 6.** Liver gene and protein expression at 22 weeks. (A) mRNA expression by RT-qPCR of main transcription factors (Chrebp-1, Srebp-1, Ppar $\alpha$ , Ppar $\gamma$ ), (B) fatty acids synthesis (Hmgcr, Soat1, Acc1, Fasn, Scd1, Dgat2), (C) uptake/efflux fatty acids (Cd36, Cd204, Fatp2, Abca1, Abcg1), (D) oxidative stress (Nrf2, Hmox-1, Sod1, Catalase, Pgc-1 $\alpha$ , Drp-1), (E) Inflammation (Ccl2, Ccl5, Cxcl10, Cx3cl1, Il-15, Tlr4), and (F) fibrosis (Tgfb $\beta$ , Ctgf, Grem1) was evaluated. Fold changes of the target gene was normalized by of their respective housekeeping gene 18s ribosomal subunit, (G) Protein expression of lipogenic enzymes by western blot was evaluated. Fold changes of proteins levels in BTBR ob/ob vs. BTBR WT (n-fold = 1) normalized by  $\beta$ -Actin and images of their respective Western Blot. Data are shown as scatter dot plots and mean  $\pm$  SEM of each group ( $n = 6$  mice/group); \*  $p < 0.05$ , \*\*  $p < 0.01$  vs. BTBR WT.

### 3. Discussion

In this study, we aimed to describe the presence of MALFD in BTBR ob/ob mice and the potential pathogenetic mechanisms involved. This model was previously approached by Lan et al. while comparing microarray profile between two experimental models of diabetes: C57BL/6J (B6) ob/ob (diabetes resistant) and BTBR ob/ob (diabetes suscepti-

ble) [24]. Although we cannot compare our results with those of Lan et al. [24] as different controls were used, our data reaffirm the importance of the genetic background in the preclinical study of diabetes complications.

The comparative advantage of the C57BL/6J ob/ob model was the higher percentage of hepatic steatosis, but hyperglycemia was only present up to 14–16 weeks of life, and then returned to euglycemia. However, the BTBR strain was characterized by hyperglycemia that was maintained over time [26,27]. Leptin deficiency in BTBR strain is a key mechanism for the acceleration of hyperglycemia-associated damage, indicating the importance of the genetic background as responsible for the modification of the diabetic phenotype [28].

The discrepancy between leptin signaling dysfunction in murine models (ob/ob and db/db mice) and the hyperleptinemia detected in obese individuals is well known [29–31]. Leptin administration reduced hepatic steatosis in ob/ob mice by restoring adipose tissue and hepatic expression of aquaglyceroporins [32]. Leptin also alters energy intake and fat mass, but not energy expenditure in lean subjects [33]. In fact, reversibility of diabetic nephropathy in BTBR ob/ob mice was noted after recombinant leptin administration [20]. In this regard, it would be of interest to study the potential beneficial effect of leptin on the reversibility of hepatic steatosis in the BTBR strain. Therefore, the role of leptin in the progression of obesity complications needs to be further investigated.

Hyperphagia observed in BTBR ob/ob leads to a 2-fold increased on daily food intake, body weight and liver weight compared to the non-diabetic control mice at 22 weeks. By clinical, analytical, and histopathological analysis, we have confirmed the presence of hepatic steatosis in early (12 weeks) and late (22 weeks) life stages of BTBR ob/ob mice. For that reason, we considered to further investigate the mechanisms involved in intrahepatic lipid accumulation, particularly whether it was merely a passive accumulation of dietary lipids or whether it was associated with DNL from carbohydrate sources and/or energy excess [34].

These mice show increased fatty acids uptake proteins and downregulation of efflux lipid transporters, both mechanisms promoting lipid accumulation in the hepatocyte. Of note, the activation of these pathways leads to the formation of monounsaturated fatty acids (C16:1n-7, C18:1n-9cis) and saturated fatty acids (C16:0 and C18:0), associated with DNL. We observed that BTBR ob/ob mice depicted abnormalities in the receptors related to influx and efflux of fatty acids, as well as on the activation of the mechanisms involved in mitochondrial dysfunction and DNL. The synergy of these factors leads to an increased ectopic accumulation of fatty acids in the liver. Additionally, in order to evaluate the effect of hyperglycemia on in liver TG and NEFA in euglycemic normal weight mice (BTBR WT), hyperglycemic/normal weight (BTBR + STZ) and hyperglycemic mice and obese mice (BTBR ob/ob).

Lipidomic analysis of intrahepatic TG and NEFA fractions showed a distinctive profile in each experimental group. Since the diet was identical in all groups, these results may suggest the existence of a different metabolic lipid synthesis rate. Of interest, the lipid profile associated with BTBR ob/ob mice showed an enrichment in de novo synthesized lipids (C16:0, C18:0, C16:1n-7 and C18:1n-9cis), a picture similar to that observed in subjects with MAFLD [35]. Meanwhile in BTBR-STZ mice there was an increase in the NEFA subfraction and a trend toward reduction of fatty acids accumulation in the triglycerides fraction. Several authors have demonstrated the inhibitory effect of NEFAs on glucose metabolism (transport, phosphorylation and oxidation), mainly by impairing insulin signaling in the muscle [36–39].

Indeed, the results obtained in this study support the idea that obesity, in a hyperglycemic context, activates intracellular signaling pathways in the liver related to the synthesis of new fatty acids. This effect, dependent on daily intake and not of diet type, may be one of the mechanisms responsible of the progression of liver steatosis in BTBR ob/ob model.

Consumption of a high-fat diet or diet-induced obesity (DIO) increases body weight, insulin resistance and macrovesicular steatosis; however, these preclinical models do not produce significant hyperglycemia. These facts demonstrate that intrahepatic lipid accumulation is caused by both liver and adipose tissue dysfunction, an effect that may be aggravated

when insulin resistance and hyperglycemia are permanent [40]. In clinical practice, it is impossible to separate lipo/glycogenic factors involved in the MAFLD progression, however, the modulation of DNL could be a good therapeutic option. For that reason, we studied the metabolic pathways altered in this pathological scenario. A reduction in the main regulators of lipid synthesis (ChREBP1 and SREBP1c) was observed, whereas PPAR $\gamma$  was overexpressed, suggesting an increase in lipid storage, as previously described [41–43]. In addition, the increased expression of enzymes related to fatty acid synthesis (ACCI, FASN and SCD-1) confirmed the data obtained by mass spectrometric analysis.

In conclusion, BTBR ob/ob mice strain constitutes an excellent experimental model of MAFLD, showing not only liver steatosis, but also recruitment of inflammatory cells, activation of inflammatory signaling pathways, oxidative stress and lipotoxicity, all them described as meta-inflammation [44]. These features are associated with the transition from steatosis to steatohepatitis, which characterize the pathological progression of MAFLD. This experimental model resembles early stages of human MAFLD and may be an excellent translational model between MAFLD, T2DM and diabetic complications [20,45–47]. Therefore, therapeutic strategies to limit cell damage and ectopic lipid accumulation, through the selective modulation of these particular intracellular signaling pathways in early stages of MAFLD, could be promising.

## 4. Materials and Methods

### 4.1. Experimental Model

In this study we studied MAFLD progression on 1) non-diabetic control mice (Black Tan and Brachyuric (BTBR WT mice), 2) diabetic and non-obese mice (BTBR mice treated with low doses streptozotocin, BTBR-STZ), 3) diabetic and obese mice (BTBR and ob/ob (leptin deficient) (BTBR.Cg-Lepob/WiscJ; RRID:IMSR\_JAX:004824). BTBR WT and BTBR ob/ob male mice were sacrificed at 4, 6, 12 and 22 weeks ( $n = 5–6$  mice/group). Standard chow diet (LASQCDiet Rod14-H) with a low-fat content (3.5%) and water ad libitum were available. Daily intake (water and food) was measured. In parallel, 12-week-old BTBR WT mice were intraperitoneally injected with low-doses of STZ (50 mg/kg) for 5 consecutive days and 10% sucrose water was supplemented to avoid hypoglycemia post-streptozotocin injection, according to the recommendations of the Animal Models Diabetic Complications Consortium (DiaComp). All mice included in BTBR-STZ group manifested glycemia  $> 300$  mg/dl for 9–10 weeks until sacrifice (22 weeks-old). All mice included in BTBR-STZ group manifested glycemia  $> 300$  mg/dl for 9–10 weeks until sacrifice (22 weeks-old) (Supplementary Figure S2).

The measurement of glycemia and body weight was made every week using a glucometer NovaPro (Nova Biomedical Iberia, Barcelona, Spain) and digital balance, respectively. Animals were euthanized under anesthesia (ketamine 100 mg/kg and xylazine 10 mg/kg). Post-anesthetic assessment, liver and blood sample for serum collection were taken. Breeding pairs BTBR heterozygotes (BTBR ob+/-) were purchased from Jackson Laboratories (Bar Harbor, ME, USA) and the colony was expanded in-house. Animals were housed at a density of four animals per cage in a controlled environment in individually ventilated cages (20–22 °C) with 12-h light–dark cycles.

In this study, there were no exclusions and no randomization was performed due to phenotypic differences between groups.

### 4.2. Biochemical Parameters

Lipid profile and liver biochemical parameters were assessed in serum, including triglycerides (TGs), total cholesterol, high-density lipoprotein cholesterol (HDL), and low-density lipoprotein cholesterol (LDL) by Friedwald formula, alanine transaminase (ALT), aspartate transaminase (AST), alkaline phosphatase (AP) and albumin. Serum was collected from femoral artery under anesthesia prior to animal sacrifice into a Vacutainer ACD blood collection tubes (Becton Dickinson and Company, Plymouth, UK). These measurements were performed in a Roche Cobas autoanalyzer's at the central laboratories of our Institution. Liver



lipids were extracted using Folch extraction (chloroform–methanol) [48], and NEFA levels, both in serum and liver extract, were measured using NEFA C enzymatic assay kit (WAKO, Neuss, Germany) as described [49]. Liver TGs content was measured using the GPO-trinder method, for which the TG colorimetric assay kit was employed following the manufacture's instructions (Cayman Chemical Company; Ann Arbor, MI, USA).

#### 4.3. Lipid Profile Determination

Fatty acid methyl esters (FAMES), TGs and non-esterified fatty acids (NEFAs) from liver were determined as follows. A weighed amount of liver from 22 weeks mice (around 20 mg) was placed in a borosilicate glass tube (previously washed with n-hexane) containing 1 mL of 0.9% sterile sodium chloride. Tissue was homogenized on ice in two 10-s series with an OMNI TH Tissue Homogenizer (Omni International, Kennesaw, GA, USA). The homogenate was spiked with 100  $\mu$ L of the internal standard (ISTDs) trionadecanoin and nonadecanoic acid (100  $\mu$ g/mL solution (10  $\mu$ g) each; Nu-Chek Prep, Elysian, MN, USA) and the lipids were extracted with 2 mL of chloroform/methanol (2:1 *v/v*). After centrifugation (5 min at 3500 rpm), the organic phase was transferred to a new borosilicate glass tube and evaporated to dryness under N<sub>2</sub> at 30 °C. TGs and NEFAs were isolated by solid-phase extraction as described in Burdge et al. [50]. Fatty acids were hydrolyzed and methylated following an adaptation of the method described by Agren et al. [51]. Briefly, 100  $\mu$ L of n-toluene and 500  $\mu$ L of boron trifluoride-methanol solution (14%) were added to the tube, which was capped and placed into a block heater (100 °C) for 60 min. After cooling, 500  $\mu$ L of distilled water and 500  $\mu$ L of n-hexane were added. The tubes were shaken for 1 min and then centrifuged for 5 min at 3500 rpm at room temperature to separate the layers. The hexane layer was placed in a test tube and evaporated to dryness under N<sub>2</sub> at 30 °C. The extracts were reconstituted with 100  $\mu$ L of n-hexane and transferred to an automatic injector vial containing a glass insert of 300  $\mu$ L.

FAMES were analyzed by gas chromatography/electron ionization mass spectrometry (GC/MSEI), using an Agilent 6890N GC equipped with an Agilent 7683 autosampler, and an Agilent 5973N mass spectrometry detector. FAMES were separated with a J&W DB-Fast FAME capillary column (30 m  $\times$  0.2 mm  $\times$  0.25  $\mu$ m film thickness) (Agilent Technologies; Santa Clara, CA, USA). The injector temperature was set at 250 °C, and 1  $\mu$ L injections were performed (split ratio 25:1). GC was run using an optimized temperature program, as follows: the program started at 50 °C, held for 0.5 min, increased to 194 °C at a rate of 25 °C/min, held for 1 min, increased to 245 °C at a rate of 5 °C/min, and held for 3 min. Helium was used as a carrier gas (14 psi, constant pressure mode). FAMES were detected using the selected ion monitoring (SIM) mode. Based on the work of Thurnhofer and Vetter [52], several *m/z* ions common to saturated, monounsaturated, and polyunsaturated FAMES were monitored. Twelve mixtures of FAME external calibration standards were prepared by diluting FAME mix certified reference material (Supelco 37 Component FAME Mix, Merck) in hexane. These standards were kept at –80 °C until analysis. 40  $\mu$ L of each mixture were added to a tube, were spiked with 100  $\mu$ L of the ISTD C19:0-methyl ester (100  $\mu$ g/mL solution (10  $\mu$ g)), evaporated to dryness under N<sub>2</sub> at 30 °C, reconstituted with 100  $\mu$ L of hexane, and transferred to an automatic injector vial containing a glass insert of 300  $\mu$ L. The equivalents of C19:0 added to the samples as TG and NEFA ISTDs were the same as the amount of C19:0-methyl ester added to the external calibrators. The concentration of FAMES in the samples were calculated by linear regression of the peak area ratio relative to that of the internal standard. The normalized concentrations were calculated by dividing the concentrations by the weight of the liver tissue.

#### 4.4. Histological Analysis and Immunohistochemistry Studies

A section of liver was fixed in 4% formaldehyde and further embedded in paraffin. 4  $\mu$ m tissue sections were stained for histochemical studies (H&E/Periodic Acid Schiff) and immunohistochemistry. The liver sections were classified according to a semiquantitative histopathological score damage (NAS, NAFLD activity score) performed by a

trained personnel in a blinded manner [53]. The primary antibodies for immunodetection were: F4/80 monocytes/macrophages ([1:70], MCA497, RRID:AB\_2098196, Bio-Rad; Hercules, CA, USA), CD3 T lymphocytes ([1:100], M7254, RRID:AB\_2631163, Agilent Technologies; Santa Clara, CA, USA), MPO ([1:100], TC66701, RRID:AB\_579628, Agilent Technologies; Santa Clara, CA, USA), phosphorylated (p-) STAT3 serine 727 ([1:100], 9134, RRID:AB\_331589, Cell Signaling Technology; Danvers, MA, USA), p-nuclear factor erythroid 2-related factor 2 (NRF2) serine 40 ([1:2000], ab76026, RRID:AB\_1524049, Abcam; Cambridge, UK) and 4-hydroxy-2-nonenal (4-HNE) ([1:200], ab46545, RRID:AB\_722490, Abcam; Cambridge, UK). All primary antibodies were assessed by indirect immunoperoxidase ([1:2000], except for p-NRF2, which incubated with the Vectastain Elite ABC HRP Kit RTU (PK-7100, RRID:AB\_2336827, Vector Laboratories; Burlingame, CA, USA). Sections were revealed with ImmPACT DAB Peroxidase Substrate (SK-4105, RRID:AB\_2336520, Vector Laboratories; Burlingame, CA, USA) and counterstained with hematoxylin (Thermo Fisher Scientific; Waltham, MA, USA). Positive staining was quantified using Image-Pro Plus software and expressed as percentage of the total area or number of positive cells (per 10 random fields).

#### 4.5. Gene Expression Studies

Total RNA from liver tissue was isolated with TRIzol G A4051 (Panreac AppliChem, Barcelona, Spain). Complementary DNA (cDNA) was synthesized by a High-Capacity cDNA Archive Kit (Applied Biosystems, Foster City, CA, USA) using 2 µg total RNA primed with random primers following the manufacturer's instructions. Quantitative gene expression analysis was performed by qRT-PCR (Quantitative real-time PCR 7500 Applied Biosystems, System SDS software V.1.2b1c3) using TaqMan gene expression assays for mouse and primers designed through Primer-BLAST software and synthesized by Thermo Fisher Scientific; Waltham, MA, USA. The expression of targets genes was analyzed in duplicate and normalized to housekeeping gene 18s rRNA. Gene expression changes are referred versus the average gene expression in BTBR WT animals (normalized as 1), therefore each gene is shown as fold change. The primers for PCR detection are listed in Supplementary Table S1.

#### 4.6. Protein Studies

Liver tissue samples were homogenized in lysis buffer (50 mM Tris-HCl, 150 mM of NaCl, 2 mM of EDTA, 2 mM of EGTA, 0.2% Triton X-100, 0.3% Igepal complemented with protease inhibitor cocktail (CP8340, Sigma-Aldrich; Saint Louis, MO, USA) and phosphatase inhibitor cocktail (P0044, Sigma-Aldrich; Saint Louis, MO, USA) and quantified using the BCA protein assay kit (Thermo Fisher Scientific; Waltham, MA, USA) to later separate the proteins (50 µg) in 8–12% acrylamide gels using SDS-PAGE. After electrophoresis, samples were transferred to PVDF membranes (IPVH00010, Millipore, Bedford, MA, USA), blocked in TBS containing 0.1% Tween 20 (TBS-T) and 5% skimmed milk for 1 h at room temperature and incubated in the same buffer with different primary antibodies overnight at 4 °C. The following primary antibodies were employed: SREBP1 ([1:500], NB600–582, RRID:AB\_10001575, Novusbio, Bio-Techne; Minneapolis, MN, USA), PPARγ (E-8) ([1:500], sc7273, RRID:AB\_628115, Santa Cruz Biotechnology; Santa Cruz, CA, USA), DGAT2 ([1:1000], ab237613, Abcam; Cambridge, UK), SCD1 (C12H5) ([1:1000, #2794S, RRID:AB\_2183099, Cell Signaling Technology; Danvers, MA, USA) and FASN (C20G5) (1:1000, #3180S, RRID:AB\_2100796, Cell Signaling Technology; Danvers, MA, USA). After that, blots were washed with TBST and incubated 1 h at room temperature with the appropriate HRP (horseradish peroxidase)-conjugated secondary antibody (anti-mouse or anti-rabbit, 1:2000 dilution, Invitrogen; Waltham, MA, USA). After being washed with TBST, blots were developed with the chemiluminescence method (ECL Luminata Crescendo, WBLUR0500, Millipore; Burlington, MA, USA) and scanned using the ImageQuant LAS-4000 (GE Healthcare; Chicago, IL, USA). Blots were then probed with mouse monoclonal anti-β-Actin antibody (1:5000 dilution, A2228, Sigma-Aldrich; Saint Louis, MO, USA) and

levels of expression were corrected for minor differences in loading. Results were quantified using Quantity One software (Bio-Rad; Hercules, CA, USA) and expressed as densitometric arbitrary units (AU).

#### 4.7. Statistical Analysis

The data are presented as scatter dot plots with mean  $\pm$  SEM (graphs) or median  $\pm$  IQR (tables) of the total number of animals. Graphs and corresponding statistical tests were carried out in R (v4.0.2) or GraphPad Prism V.6 software (GraphPad Software Inc., La Jolla, CA, USA). Statistical analyses were performed using Student's *t* or non-parametric Mann-Whitney *U* test for comparison between two groups. Lipid discriminant and clustering analysis was carried out using respectively an Orthogonal Partial Least Squares Discriminant Analysis (oPLS-DA) and a Euclidean Hierarchical clustering with the MetaboAnalystR 2.0 package [53]. Differences were considered statistically significant at  $p < 0.05$ .

**Supplementary Materials:** The following supporting information can be downloaded at: <https://www.mdpi.com/article/10.3390/ijms23073965/s1>.

**Author Contributions:** S.M.-F. and J.E. are the guarantors of this work and, as such, had full access to all the data in the study and takes responsibility for the integrity of the data and the accuracy of the data analysis. L.O.-R. and M.S.-C. contributed to the conception, design, performance of the experiments; acquisition, analysis, interpretation of all data and drafting of the manuscript for the study. M.O., I.L., A.S.-V. and L.J.-C. contributed to the performance of the experiments, acquisition, analysis and interpretation of data. J.A.M., S.M.-F. and J.E., contributed to interpretation of the data, drafting and critical review of the manuscript, and in securing financial support for the study. All authors have read and agreed to the published version of the manuscript.

**Funding:** This research was funded by Instituto de Salud Carlos III (PI17/00130, PI20/00375, PI20/00487; and DTS19/00093 (Co-funded by European Regional Development Fund/European Social Fund "A way to make Europe"/"Investing in your future"), Spanish Biomedical Research Centre in Cardiovascular Diseases (CIBERCV), Consejería de Salud y Familias-FEDER, Junta de Andalucía (PIGE-0052-2020), Consejería de Economía, Conocimiento, Empresas y Universidad (1381179-R) and Spanish Society of Nephrology (SEN). The Spanish Ministry of Science and Innovation/State Investigation Agency (10.13039/501100011033) supported the salary of JAM (RYC-2017-22369, Co-funded by European Regional Development Fund/European Social Fund "A way to make Europe"/"Investing in your future").

**Institutional Review Board Statement:** Animal studies were approved by the FISS-FJD Animal Experimentation Ethics Committee and by the Madrid regional government (Ref. PROEX 079/18). All animal procedures were conformed to EU Directive 2010/63EU and Real Decreto 53/2013 regarding protection of animals used for experimental and other scientific purposes.

**Informed Consent Statement:** Not applicable.

**Data Availability Statement:** The database of the measurements and analytics will be available on request.

**Acknowledgments:** The authors are grateful to Sergio Mezzano (Laboratorio de Nefrología, Facultad de Medicina, Universidad Austral de Chile, Valdivia, Chile), Gabriel Mezzano (Departamento de Medicina, Sección Gastroenterología, Hospital del Salvador, Escuela de Medicina Universidad de Chile) and Carmen Gomez-Guerrero (IIS-Fundación Jiménez Díaz, Madrid) for clinical and technical support in the development of this research.

**Conflicts of Interest:** The authors declare no conflict of interest.

## References

1. Sberna, A.L.; Bouillet, B.; Rouland, A.; Brindisi, M.C.; Nguyen, A.; Mouillot, T.; Duvillard, L.; Denimal, D.; Loffroy, R.; Vergès, B.; et al. European Association for the Study of the Liver (EASL), European Association for the Study of Diabetes (EASD) and European Association for the Study of Obesity (EASO) clinical practice recommendations for the management of non-alcoholic fatty liver diseases. *Diabet. Med.* **2018**, *35*, 368–375. [[CrossRef](#)] [[PubMed](#)]
2. European Association for the Study of the Liver (EASL); European Association for the Study of Diabetes (EASD); European Association for the Study of Obesity (EASO). EASL–EASD–EASO Clinical Practice Guidelines for the management of non-alcoholic fatty liver disease. *J. Hepatol.* **2016**, *64*, 1388–1402. [[CrossRef](#)] [[PubMed](#)]
3. Younossi, Z.M.; Koenig, A.B.; Abdelatif, D.; Fazel, Y.; Henry, L.; Wymer, M. Global epidemiology of nonalcoholic fatty liver disease—Meta-analytic assessment of prevalence, incidence, and outcomes. *Hepatology* **2016**, *64*, 73–84. [[CrossRef](#)] [[PubMed](#)]
4. Younossi, Z.M.; Blissett, D.; Blissett, R.; Henry, L.; Stepanova, M.; Younossi, Y.; Racila, A.; Hunt, S.; Beckerman, R. The economic and clinical burden of nonalcoholic fatty liver disease in the United States and Europe. *Hepatology* **2016**, *64*, 1577–1586. [[CrossRef](#)]
5. Targher, G.; Corey, K.E.; Byrne, C.D.; Roden, M. The complex link between NAFLD and type 2 diabetes mellitus—Mechanisms and treatments. *Nat. Rev. Gastroenterol. Hepatol.* **2021**, *18*, 599–612. [[CrossRef](#)]
6. Younossi, Z.M. Non-alcoholic fatty liver disease—A global public health perspective. *J. Hepatol.* **2019**, *70*, 531–544. [[CrossRef](#)]
7. Lonardo, A.; Lugari, S.; Ballestri, S.; Nascimbeni, F.; Baldelli, E.; Maurantonio, M. A round trip from nonalcoholic fatty liver disease to diabetes: Molecular targets to the rescue? *Acta Diabetol.* **2018**, *56*, 385–396. [[CrossRef](#)]
8. Lonardo, A.; Nascimbeni, F.; Mantovani, A.; Targher, G. Hypertension, diabetes, atherosclerosis and NASH: Cause or consequence? *J. Hepatol.* **2018**, *68*, 335–352. [[CrossRef](#)]
9. Mantovani, A.; Petracca, G.; Beatrice, G.; Tilg, H.; Byrne, C.D.; Targher, G. Non-alcoholic fatty liver disease and risk of incident diabetes mellitus: An updated meta-analysis of 501,022 adult individuals. *Gut* **2021**, *70*, 962–969. [[CrossRef](#)]
10. Sung, K.C.; Jeong, W.S.; Wild, S.H.; Byrne, C.D. Combined Influence of Insulin Resistance, Overweight/Obesity, and Fatty Liver as Risk Factors for Type 2 Diabetes. *Diabetes Care* **2012**, *35*, 717–722. [[CrossRef](#)]
11. Gastaldelli, A. Insulin resistance and reduced metabolic flexibility: Cause or consequence of NAFLD? *Clin. Sci.* **2017**, *131*, 2701–2704. [[CrossRef](#)]
12. Eslam, M.; Newsome, P.N.; Sarin, S.K.; Anstee, Q.M.; Targher, G.; Romero-Gomez, M.; Zelber-Sagi, S.; Wai-Sun Wong, V.; Dufour, J.F.; Schattenberg, J.M.; et al. A new definition for metabolic dysfunction-associated fatty liver disease: An international expert consensus statement. *J. Hepatol.* **2020**, *73*, 202–209. [[CrossRef](#)]
13. Sutti, S.; Albano, E. Adaptive immunity: An emerging player in the progression of NAFLD. *Nat. Rev. Gastroenterol. Hepatol.* **2019**, *17*, 81–92. [[CrossRef](#)]
14. McPherson, S.; Hardy, T.; Henderson, E.; Burt, A.D.; Day, C.P.; Anstee, Q.M. Evidence of NAFLD progression from steatosis to fibrosing-steatohepatitis using paired biopsies: Implications for prognosis and clinical management. *J. Hepatol.* **2015**, *62*, 1148–1155. [[CrossRef](#)]
15. Le Garf, S.; Nègre, V.; Anty, R.; Gual, P. Metabolic Fatty Liver Disease in Children: A Growing Public Health Problem. *Biomedicines* **2021**, *9*, 1915. [[CrossRef](#)]
16. Eslam, M.; Alkhoury, N.; Vajro, P.; Baumann, U.; Weiss, R.; Socha, P.; Marcus, C.; Lee, W.S.; Kelly, D.; Porta, G.; et al. Defining paediatric metabolic (dysfunction)-associated fatty liver disease: An international expert consensus statement. *Lancet. Gastroenterol. Hepatol.* **2021**, *6*, 864–873. [[CrossRef](#)]
17. Morandi, A.; Di Sessa, A.; Zusi, C.; Umamo, G.R.; El Mazloum, D.; Fornari, E.; del Giudice, E.M.; Targher, G.; Maffei, C. Nonalcoholic Fatty Liver Disease and Estimated Insulin Resistance in Obese Youth: A Mendelian Randomization Analysis. *J. Clin. Endocrinol. Metab.* **2020**, *105*, e4046–e4054. [[CrossRef](#)]
18. Monserrat-Mesquida, M.; Quetglas-Llabrés, M.; Abbate, M.; Montemayor, S.; Mascaró, C.M.; Casares, M.; Tejada, S.; Abete, I.; Zulet, M.A.; Tur, J.A.; et al. Oxidative Stress and Pro-Inflammatory Status in Patients with Non-Alcoholic Fatty Liver Disease. *Antioxidants* **2020**, *9*, 759. [[CrossRef](#)]
19. Oligschlaeger, Y.; Shiri-Sverdlov, R. NAFLD Preclinical Models: More than a Handful, Less of a Concern? *Biomedicines* **2020**, *8*, 28. [[CrossRef](#)]
20. Hudkins, K.L.; Pichaiwong, W.; Wietecha, T.; Kowalewska, J.; Banas, M.C.; Spencer, M.W.; Mühlfeld, A.; Koelling, M.; Pippin, J.W.; Shankland, S.J.; et al. BTBR Ob/Ob mutant mice model progressive diabetic nephropathy. *J. Am. Soc. Nephrol. JASN* **2010**, *21*, 1533–1542. [[CrossRef](#)]
21. Keller, M.P.; Choi, Y.J.; Wang, P.; Davis, D.B.; Rabaglia, M.E.; Oler, A.T.; Stapleton, D.S.; Argmann, C.; Schueler, K.L.; Edwards, S.; et al. A gene expression network model of type 2 diabetes links cell cycle regulation in islets with diabetes susceptibility. *Genome Res.* **2008**, *18*, 706–716. [[CrossRef](#)] [[PubMed](#)]
22. Clee, S.M.; Attie, A.D. The Genetic Landscape of Type 2 Diabetes in Mice. *Endocr. Rev.* **2007**, *28*, 48–83. [[CrossRef](#)] [[PubMed](#)]
23. Bhatnagar, S.; Oler, A.T.; Rabaglia, M.E.; Stapleton, D.S.; Schueler, K.L.; Truchan, N.A.; Worzella, S.L.; Stoehr, J.P.; Clee, S.M.; Yandell, B.S.; et al. Positional Cloning of a Type 2 Diabetes Quantitative Trait Locus; Tomosyn-2, a Negative Regulator of Insulin Secretion. *PLoS Genet.* **2011**, *7*, e1002323. [[CrossRef](#)] [[PubMed](#)]
24. Lan, H.; Rabaglia, M.E.; Stoehr, J.P.; Nadler, S.T.; Schueler, K.L.; Zou, F.; Yandell, B.S.; Attie, A.D. Gene Expression Profiles of Nondiabetic and Diabetic Obese Mice Suggest a Role of Hepatic Lipogenic Capacity in Diabetes Susceptibility. *Diabetes* **2003**, *52*, 688–700. [[CrossRef](#)] [[PubMed](#)]



25. Sobczak, A.I.S.; Pitt, S.J.; Smith, T.K.; Ajjan, R.A.; Stewart, A.J. Lipidomic profiling of plasma free fatty acids in type-1 diabetes highlights specific changes in lipid metabolism. *Biochim. Biophys. Acta. Mol. Cell Biol. Lipids* **2021**, *1866*, 158823. [[CrossRef](#)]
26. Lavozy, C.; Rodrigues-Diez, R.R.; Plaza, A.; Carpio, D.; Egido, J.; Ruiz-Ortega, M.; Mezzano, S. VEGFR2 Blockade Improves Renal Damage in an Experimental Model of Type 2 Diabetic Nephropathy. *J. Clin. Med.* **2020**, *9*, 302. [[CrossRef](#)]
27. Moreno, J.A.; Gomez-Guerrero, C.; Mas, S.; Sanz, A.B.; Lorenzo, O.; Ruiz-Ortega, M.; Opazo, L.; Mezzano, S.; Egido, J. Targeting inflammation in diabetic nephropathy: A tale of hope. *Expert Opin Investig Drugs*. **2018**, *27*, 917–930. [[CrossRef](#)]
28. Haluzik, M.; Colombo, C.; Gavriloiva, O.; Chua, S.; Wolf, N.; Chen, M.; Stannard, B.; Dietz, K.R.; Le Roith, D.; Reitman, M.L. Genetic Background (C57BL/6J Versus FVB/N) Strongly Influences the Severity of Diabetes and Insulin Resistance in ob/ob Mice. *Endocrinology* **2004**, *145*, 3258–3264. [[CrossRef](#)]
29. Knight, Z.A.; Hannan, K.S.; Greenberg, M.L.; Friedman, J.M. Hyperleptinemia Is Required for the Development of Leptin Resistance. *PLoS ONE* **2010**, *5*, e11376. [[CrossRef](#)]
30. Mittendorfer, B.; Horowitz, J.F.; DePaoli, A.M.; McCamish, M.A.; Patterson, B.W.; Klein, S. Recombinant Human Leptin Treatment Does Not Improve Insulin Action in Obese Subjects With Type 2 Diabetes. *Diabetes* **2011**, *60*, 1474. [[CrossRef](#)]
31. Leon-Cabrera, S.; Solís-Lozano, L.; Suárez-Álvarez, K.; González-Chávez, A.; Béjar, Y.L.; Robles-Díaz, G.; Escobedo, G. Hyperleptinemia is associated with parameters of low-grade systemic inflammation and metabolic dysfunction in obese human beings. *Front. Integr. Neurosci.* **2013**, *7*, 62. [[CrossRef](#)]
32. Rodríguez, A.; Moreno, N.R.; Balaguer, I.; Méndez-Giménez, L.; Becerril, S.; Catalán, V.; Gómez-Ambrosi, J.; Portincasa, P.; Calamita, G.; Soveral, G.; et al. Leptin administration restores the altered adipose and hepatic expression of aquaglyceroporins improving the non-alcoholic fatty liver of ob/ob mice. *Sci. Rep.* **2015**, *5*, 1–13. [[CrossRef](#)]
33. Chrysafi, P.; Perakakis, N.; Farr, O.; Stefanakis, K.; Peradze, N.; Sala-Vila, A.; Mantzoros, C. Leptin alters energy intake and fat mass but not energy expenditure in lean subjects. *Nat. Commun.* **2020**, *11*, 5145. [[CrossRef](#)]
34. Neuschwander-Tetri, B.A. Non-alcoholic fatty liver disease. *BMC Med.* **2017**, *15*, 97–113. [[CrossRef](#)]
35. Smith, G.I.; Shankaran, M.; Yoshino, M.; Schweitzer, G.G.; Chondronikola, M.; Beals, J.W.; Okunade, A.L.; Patterson, B.W.; Nyangau, E.; Field, T.; et al. Insulin resistance drives hepatic de novo lipogenesis in nonalcoholic fatty liver disease. *J. Clin. Investig.* **2020**, *130*, 1453. [[CrossRef](#)]
36. Dresner, A.; Laurent, D.; Marcucci, M.; Griffin, M.E.; Dufour, S.; Cline, G.W.; Slezak, L.A.; Andersen, D.K.; Hundal, R.S.; Rothman, D.L.; et al. Effects of free fatty acids on glucose transport and IRS-1-associated phosphatidylinositol 3-kinase activity. *J. Clin. Investig.* **1999**, *103*, 253. [[CrossRef](#)]
37. Bergman, R.N. Non-esterified fatty acids and the liver: Why is insulin secreted into the portal vein? *Diabetologia* **2000**, *43*, 946–952. [[CrossRef](#)]
38. Everett-Grueter, C.; Edgerton, D.S.; Donahue, E.P.; Vaughan, S.; Chang, A.C.; Sindelar, D.K.; Cherrington, A.D. The effect of an acute elevation of NEFA concentrations on glucagon-stimulated hepatic glucose output. *Am. J. Physiol.—Endocrinol. Metab.* **2006**, *291*, 449–459. [[CrossRef](#)]
39. Kehlenbrink, S.; Koppaka, S.; Martin, M.; Relwani, R.; Cui, M.-H.; Hwang, J.-H.; Li, Y.; Basu, R.; Hawkins, M.; Kishore, P. Elevated NEFA levels impair glucose effectiveness by increasing net hepatic glycogenolysis. *Diabetologia* **2012**, *55*, 3021. [[CrossRef](#)]
40. Duval, C.; Thissen, U.; Keshtkar, S.; Accart, B.; Stienstra, R.; Boekschoten, M.V.; Roskams, T.; Kersten, S.; Müller, M. Adipose Tissue Dysfunction Signals Progression of Hepatic Steatosis Towards Nonalcoholic Steatohepatitis in C57Bl/6 Mice. *Diabetes* **2010**, *59*, 3181. [[CrossRef](#)] [[PubMed](#)]
41. Liss, K.H.H.; Finck, B.N. PPARs and Nonalcoholic Fatty Liver Disease. *Biochimie* **2017**, *136*, 65. [[CrossRef](#)] [[PubMed](#)]
42. Nakamuta, M.; Kohjima, M.; Morizono, S.; Kotoh, K.; Yoshimoto, T.; Miyagi, I.; Enjoji, M. Evaluation of fatty acid metabolism-related gene expression in nonalcoholic fatty liver disease. *Int. J. Mol. Med.* **2005**, *16*, 631–635. [[PubMed](#)]
43. Gavriloiva, O.; Haluzik, M.; Matsusue, K.; Cutson, J.J.; Johnson, L.; Dietz, K.R.; Nicol, C.J.; Vinson, C.; Gonzalez, F.J.; Reitman, M.L. Liver Peroxisome Proliferator-activated Receptor  $\gamma$  Contributes to Hepatic Steatosis, Triglyceride Clearance, and Regulation of Body Fat Mass. *J. Biol. Chem.* **2003**, *278*, 34268–34276. [[CrossRef](#)] [[PubMed](#)]
44. Gehrke, N.; Schattenberg, J.M. Metabolic Inflammation—A Role for Hepatic Inflammatory Pathways as Drivers of Comorbidities in Nonalcoholic Fatty Liver Disease? *Gastroenterology* **2020**, *158*, 1929–1947.e6. [[CrossRef](#)]
45. Friedman, S.L.; Neuschwander-Tetri, B.A.; Rinella, M.; Sanyal, A.J. Mechanisms of NAFLD development and therapeutic strategies. *Nat. Med.* **2018**, *24*, 908–922. [[CrossRef](#)]
46. Sheka, A.C.; Adeyi, O.; Thompson, J.; Hameed, B.; Crawford, P.A.; Ikramuddin, S. Nonalcoholic Steatohepatitis: A Review. *JAMA* **2020**, *323*, 1175–1183. [[CrossRef](#)]
47. Lee, V.K.; Hosking, B.M.; Holeniewska, J.; Kubala, E.C.; Lundh von Leithner, P.; Gardner, P.J.; Foxton, R.H.; Shima, D.T. BTBR ob/ob mouse model of type 2 diabetes exhibits early loss of retinal function and retinal inflammation followed by late vascular changes. *Diabetologia* **2018**, *61*, 2422–2432. [[CrossRef](#)]
48. Minniti, M.E.; Ahmed, O.; Pedrelli, M. Enzymatic Quantification of Liver Lipids after Folch Extraction. *Methods Mol. Biol.* **2020**, *2164*, 101–108.
49. Mas, S.; Martínez-Pinna, R.; Martín-Ventura, J.L.; Pérez, R.; Gomez-Garre, D.; Ortiz, A.; Fernandez-Cruz, A.; Vivanco, F.; Egido, J. Local Non-Esterified Fatty Acids Correlate With Inflammation in Atheroma Plaques of Patients With Type 2 Diabetes. *Diabetes* **2010**, *59*, 1292. [[CrossRef](#)]

50. Burdge, G.C.; Wright, P.; Jones, A.E.; Wootton, S.A. A method for separation of phosphatidylcholine, triacylglycerol, non-esterified fatty acids and cholesterol esters from plasma by solid-phase extraction. *Br. J. Nutr.* **2000**, *84*, 781–787. [[CrossRef](#)]
51. Agren, J.; Julkunen, A.; Penttilä, I. Rapid separation of serum lipids for fatty acid analysis by a single aminopropyl column. *J. Lipid Res.* **1992**, *33*, 1871–1876. [[CrossRef](#)]
52. Thurnhofer, S.; Vetter, W. A Gas Chromatography/Electron Ionization–Mass Spectrometry–Selected Ion Monitoring Method for Determining the Fatty Acid Pattern in Food after Formation of Fatty Acid Methyl Esters. *J. Agric. Food Chem.* **2005**, *53*, 8896–8903. [[CrossRef](#)] [[PubMed](#)]
53. Kleiner, D.E.; Brunt, E.M.; Van Natta, M.; Behling, C.; Contos, M.J.; Cummings, O.W.; Ferrell, L.D.; Liu, Y.-C.; Torbenson, M.S.; Unalp-Arida, A.; et al. Design and validation of a histological scoring system for nonalcoholic fatty liver disease. *Hepatology* **2005**, *41*, 1313–1321. [[CrossRef](#)] [[PubMed](#)]